

High-throughput snapshot spectral imaging in two dimensions

Andrew R Harvey and David W Fletcher-Holmes
Electrical, Electronic and Computer Engineering, School of Physical Sciences, Heriot Watt
University, Riccarton, Edinburgh, EH14 4AS UK

ABSTRACT

We describe demonstrations of two new techniques for snapshot spectral imaging in two dimensions. The first, based on a generalisation of the Lyot filter, we believe to be the first technique able to spectrally image in snapshot mode with modest resolution and without the need for data inversion. The second demonstration is of a biologically inspired foveal hyperspectral imager, which mitigates the data acquisition and processing bottleneck encountered in traditional hyperspectral imaging approaches.

1. INTRODUCTION

Over the years many spectral imaging techniques have been described and it has become clear that all techniques involve some compromise with no single technique offering a panacea¹. The ideal technique can be determined by a comparison of the requirements for an application and the capabilities of candidate techniques. In this paper we describe two novel approaches that offer the important and fundamental advantages of snapshot spectral imaging in two dimensions. The first, dubbed IRIS², enables 2D spectral imaging with modest spectral resolution and modest field of view. The second, biologically inspired technique, offers high spectral resolution in a small 2D fovea that is surrounded by a panchromatic periphery that offers situational awareness. To highlight the advantages offered by these new techniques we will first discuss the limitations of traditional approaches to spectral imaging.

A fundamental aim of spectral imaging is to record a three-dimensional spectral-image cube (two transverse image dimensions and one spectral dimension) and a fundamental issue to be tackled is that this must be recorded using two-dimensional detector arrays. The solution to this dilemma is normally to time-sequentially record snapshot images of two of the spectral cube dimensions and to reconstruct the third dimension of the spectral data cube from *post hoc* assembly of the time-sequential data. Two pertinent examples are the use of a time-sequential filter wheel and the one-dimensional, pushbroom-scanned spectral imager¹. In the former case a time-sequential series of narrow-band images are recorded and subsequently coregistered and assembled into a spectral data cube. In the latter case, a time-sequential series of one-dimensional snapshot spectral images are recorded and reassembled to form a two-dimensional spectral image.

A major disadvantage of both techniques is that they are fundamentally unsuitable for recording phenomena that are changing on a timescale that is shorter than the duration required to reconstruct the data cube. Since this will typically be tens or hundreds of detector frames this is a major and fundamental restriction that imposes severe limitations in the application of spectral imaging to, for example, fast biochemical and combustion processes. Further problems arise when there is mutual translation between the scene to be spectrally imaged and the imager as occurs in spectral imaging of the eye^{3,4,5,6} and spectral imaging surveillance from aerial platforms^{7,8,9,10,11}. In both cases the major problem occurs because the translation is irregular and this can cause accurate coregistration of spectral images to be highly problematic. In the case where a one-dimensional image is scanned across the scene a penalty for imperfect coregistration is artefacts in the geometry of the spectral image, but for the case where the spectra are recorded in time sequence, imperfectly coregistered images introduce artefacts in the spectrum that reduce the effectiveness of spectral processing algorithms. In fact, to avoid this degradation typically requires coregistration of constituent images to be 1/20 of a pixel or better¹. This can be somewhat challenging. A major advantage of using a one-dimensional dispersive spectral imager, as has been demonstrated in aerial hyperspectral surveillance and spectral imaging of the eye, is that this technique does not suffer from temporally induced spectral misregistration.

A further disadvantage of recording the spectral cube in time sequence is the reduced optical throughput. If N spectral filters are employed to time-sequentially record a spectral data cube during an integration time τ the integration time available for each image is τ/N and the optical throughput is therefore reduced by a factor N . For a push-broom scanned one-dimensional spectral imager, a one-dimensional scene is recorded in a snapshot with, in principle, no multiplex loss, but to construct an image of $P \times Q$ pixels from Q such 1D images during an integration time τ means that the time available to record each 1D image is τ/Q . In this case the optical throughput is reduced by a factor Q .

We describe here two snapshot 2D spectral imaging techniques. The ability to record the full spectral data cubes in a snapshot offers the following advantages:

- Time-resolved spectral imaging of transient phenomena is possible
- No temporally induced spectral misregistration or geometric distortion is introduced
- There are no multiplex losses so signal throughput can be very high
- There are no moving parts so reliability and robustness is high

The ability to record 2D snapshot spectral images is a fundamental advantage in terms of its ability to record transient or time-varying scenes, however the multiplex advantage depends upon the application. Fundamentally, the number of pixels in the spectral image cube (that is voxels) that can be recorded in a snapshot is limited by the space-bandwidth product (that is, the number of detector pixels) of the detector array or arrays that are used. The first of the techniques we describe (IRIS) involves the snapshot imaging of M narrow-band non-overlapping images onto a single detector array so that there is a trade off between spectral resolution and field of view. The second, foveal, approach records high spectral resolution images within only the fovea and with no more image pixels in total than the maximum width, P , in pixels of the detector array and maximum number of spectral bins for each image pixel is limited by the maximum height, Q , of the detector array. The field of view for both of these techniques is limited, but if it is large enough without the need for spatial scanning for a particular application then there is a very significant multiplex advantage over other techniques. If, however, a need for an extended field of regard requires scanning of the imager than this is in effect spatial multiplexing and the full multiplex advantage will not be obtained.

2. IMAGE REPLICATION IMAGING SPECTROMETER: IRIS

The Lyot filter^{12,13,14,15}, as used for many years in astronomy, employs polarising interferometry within multiple waveplates to yield a narrow-band filter suitable for recording monochromatic images. Light not transmitted by the Lyot filter is absorbed by film polarisers. We describe here a generalisation of the Lyot filter in which Wollaston prism polarising beam splitters are used in place of film polarising enabling spectral images to be recorded simultaneously in several pass-bands without rejection of light. In describing its principle of operation we will first consider the principle of a conventional Lyot filter.

A Lyot filter, as illustrated in Figure 1 is composed of multiple waveplates sandwiched between co-aligned linear polarisers aligned to pass light polarised at 45° to the fast axis of each waveplate. The linearly polarised light propagating through the waveplate is resolved into orthogonally polarised components that interfere at the output analysing polariser with a mutual optical path difference $\Delta=(n_o-n_e)t$ between the orthogonal components where n_o and n_e are the ordinary and extraordinary refractive indices of the waveplate and t is its thickness. The output polariser is aligned with the input polariser so that the overall transmission function of the polariser-waveplate-polariser assembly is proportional to $\cos^2(\pi\nu\Delta)$ where $\nu=1/\lambda$ is optical frequency. A Lyot filter consists of an assembly of multiple polariser/waveplate combinations where the ratio between the thicknesses of consecutive waveplates is a factor of two. The spectral transmission function of an n -waveplate Lyot filter is thus the product of the transmission functions of all constituent waveplate/polariser assembly and is given by

$$T(\nu) = \prod_{i=1}^n \cos^2(i\pi\nu\Delta).$$

(1)

A four-waveplate Lyot filter is depicted in Figure 1. A similar technique is employed with the IRIS concept described here except that the film polarisers are replaced with Wollaston prism polarising beam splitters as shown Figure 2. The use of a polarising beam splitter means that after transmission through each waveplate the light is resolved into polarisations both aligned to and orthogonal to the input polarisation state. As with the Lyot filter, for the co-polarised component the transmission function is given by $\cos^2(\pi\nu\Delta)$. For the cross-polarised component the transmission function is $\sin^2(\pi\nu\Delta)$. Furthermore, these two orthogonally polarised components are displaced in angle by the beam-splitting action of the Wollaston prism and this enables two spatially separated and spectrally filtered replica images to be formed. As with the Lyot filter, subsequent Wollaston prism polariser pairs further spectrally filter and replicate the images. After transmission through n Wollaston prism polariser pairs 2^n replicated images are formed, each with a unique product of $\sin^2(i\pi\nu\Delta)$ and $\cos^2(i\pi\nu\Delta)$ transmission functions. It can be seen then that the IRIS technique simultaneously replicates the image of the image formed at the field stop whilst applying a unique spectral filtering function to each image that is determined by the order in which light arriving at each image was steered through the instrument. IRIS thus performs the function of an imaging spectral demultiplexor with image components lying within a

spectral band tending to be steered to a particular part of the detector array. The images at the detector array are prevented from overlapping by the field stop.

In general, the transmission function for each image at location j in the image plane can be written as

$$T_j(\nu) = \prod_{i=1}^n \Omega_{i, \text{pol}(i,j)}(i\pi\nu\Delta) \quad (2)$$

where

$$\begin{aligned} \Omega_{i, \text{pol}(i,j)=\text{co}}(i\pi\nu\Delta) &= \cos^2(i\pi\nu\Delta) \\ \Omega_{i, \text{pol}(i,j)=\text{cr}}(i\pi\nu\Delta) &= \Omega_{i, \text{vh}}(i\pi\nu\Delta) = \sin^2(i\pi\nu\Delta) \end{aligned} \quad (3)$$

represent the transmission functions for co-polar and cross-polar transmission through a waveplate i sandwiched between polarisers and the appropriate co-polar and cross-polar transmission functions are chosen so as to produce a spectrally filtered image at location j in the image plane. The spectrum associated with each individual image replication is determined by the geometry and order of the Wollaston prisms and waveplates. Since spectral filtering and image replication operations commute, the order of the devices is not important; it will always result in the same combination of 2^n products of the n pairs of \cos^2 and \sin^2 being applied at the image. For an IRIS employing three Wollaston prisms the eight pass-bands pass-band are given by

$$\begin{aligned} T_1(\nu) &= \cos^2[\pi\nu\Delta] \cos^2[2\pi\nu\Delta] \cos^2[4\pi\nu\Delta] \\ T_2(\nu) &= \cos^2[\pi\nu\Delta] \cos^2[2\pi\nu\Delta] \sin^2[4\pi\nu\Delta] \\ T_3(\nu) &= \cos^2[\pi\nu\Delta] \sin^2[2\pi\nu\Delta] \cos^2[4\pi\nu\Delta] \\ T_4(\nu) &= \cos^2[\pi\nu\Delta] \sin^2[2\pi\nu\Delta] \sin^2[4\pi\nu\Delta] \\ T_5(\nu) &= \sin^2[\pi\nu\Delta] \cos^2[2\pi\nu\Delta] \cos^2[4\pi\nu\Delta] \\ T_6(\nu) &= \sin^2[\pi\nu\Delta] \cos^2[2\pi\nu\Delta] \sin^2[4\pi\nu\Delta] \\ T_7(\nu) &= \sin^2[\pi\nu\Delta] \sin^2[2\pi\nu\Delta] \cos^2[4\pi\nu\Delta] \\ T_8(\nu) &= \sin^2[\pi\nu\Delta] \sin^2[2\pi\nu\Delta] \sin^2[4\pi\nu\Delta] \end{aligned} \quad (4)$$

As can be seen the first term is to the spectral transmission function of the equivalent Lyot filter. Due to the wide spectral range of IRIS it is necessary to use the dispersive variation of Δ with wavenumber when evaluating (4). In Figure 3(a) are shown the eight calculated transmission functions for an eight-band IRIS employing mica waveplates with thicknesses for the three waveplates of $t=46.86, 93.72$ and $187.44 \mu\text{m}$. The resultant pass-bands are bell-shaped and exhibit significant sidelobes. Variation of the thicknesses of the waveplates enables the form of the pass-bands to be modified to achieve specific features; for example, for operation in the $18,000$ to $28,000 \text{ cm}^{-1}$ range, optimisation to maximise the energy in each of the eight main lobes whilst minimising the energy in the sidelobes yields thickness $t=47.79, 96.57$ and $113.00 \mu\text{m}$ and the optimised spectral transmission functions are shown in Figure 3(b).

Whilst it is not possible to synthesis the contiguous rectangular functions typically employed in spectrometry, in many cases this will not significantly reduce spectral discrimination performance of IRIS. A heuristic illustration of this is the good spectral discrimination possible with the human visual system which also employs broad overlapping and bell-shaped response curves. A more quantitative appraisal is the evaluation of the separation of recorded spectra in spectral space. For example, in Figure 4 is shown the relative energy in each spectral bin when the spectra of aluminium, green paint, concrete and coniferous vegetation are convolved with rectangular response functions and also when the spectra are convolved with the response functions of IRIS. The total intensities in each bin are normalised to that of aluminium in band 8 when rectangular contiguous filters are used. Perhaps the most striking feature is that the intensity at the detectors is eight-fold higher for IRIS than for a conventional time-sequential systems. On the other hand, the bell-shaped responses of IRIS have resulted in some smoothing of the recorded spectra. In practice, the ability to discriminate between spectra is determined by both the separation of these spectra in eight-dimensional spectral space and the noise

contribution at each point. In this example, the mean reduction in separation of the spectra in spectral space is 8%, whilst the signal level is increased by a factor of eight, consequently for detector-noise limited imaging, IRIS offers a 7.4-fold improvement in signal-to-noise ratio over an ideal time-sequential spectral imager.

As a proof-of-concept illustration of the technique, we show in Figure 5 the replicated images formed at the detector plane for an input scene consisting of six coloured pens. The variations of the grey levels for each pen in the eight images is due to the filtering functions of the IRIS system. The spectral image cube is constructed by coregistration of these eight bandpass images. There are some aspects of this process that require calibration, including small amounts of fixed distortion introduced by the lens and a small amount of image smear introduced by dispersion in the Wollaston prism birefringence. Although we have demonstrated the IRIS technique in the visible band we have identified birefringent materials that will enable its applications across a wide range of wavelengths between 200 nm and 15 μm .

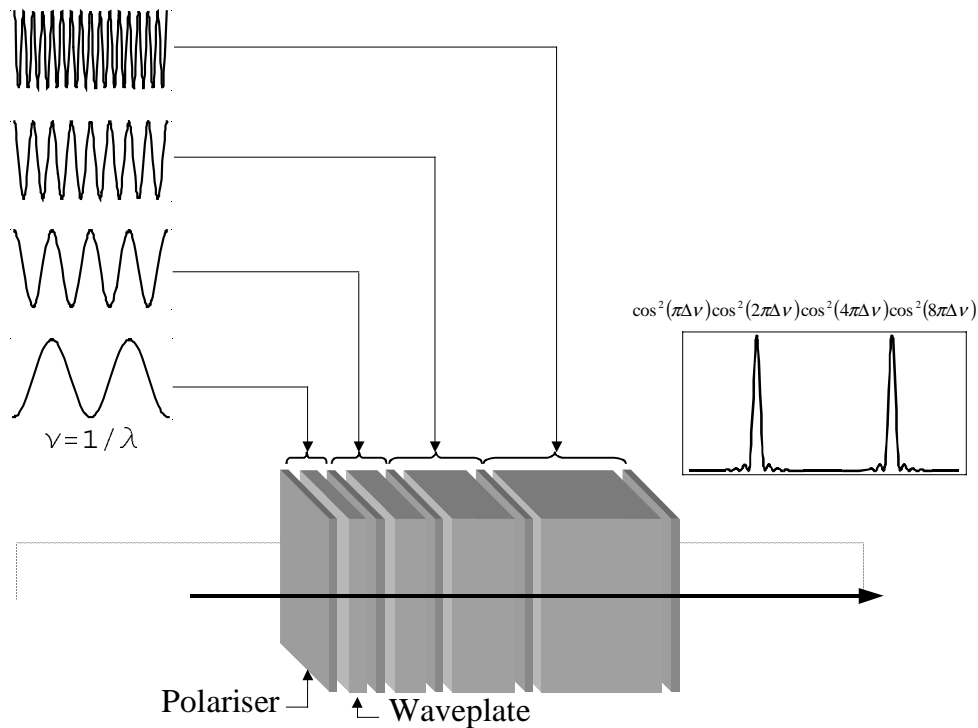


Figure 1 Depiction of the principle of operation of the Lyot filter

3. FOVEAL, SNAPSHOT HYPERSPECTRAL IMAGING

Wide field-of-view hyperspectral imaging in which a complete spectral data cube is recorded at video frame rates is likely to remain beyond technological capabilities for some time. Simple calculations indicate that such a device would involve data rates of giga-voxels per second. This not only exceeds the pixels rates of imaging detectors, but also exceeds the ability of realistic computational power to process the data. In humans, a foveal imaging system has evolved that provides the benefits of high performance colour vision but with massively reduced cost in terms of the detector (retinal) complexity and required processing power (visual cortex). High acuity and the best spectral discrimination performance colour vision is provided only in a foveal patch subtending about 10 milliradians and with less than 100 pixels across its width. Within the fovea there are only the three colour receptor cones and outwith this area exist panchromatic rods in addition to a much lower density of trichromatic cones. In operation the human eye is scanned such that the main areas of interest are imaged onto the fovea in time sequence and cuing of the regions of interest arises from images formed in the periphery with lower spatial and spectral acuity. It is reasonable to assume that evolution has optimised this system in terms of a trade of the biological cost of a high performance imaging and data processing system against the ability to detect, recognise and identify opportunities and threats. In this section we report the demonstration of a foveal hyperspectral imager that records real-time hyperspectral imagery within a two-dimensional hyperspectral fovea within a panchromatic periphery.

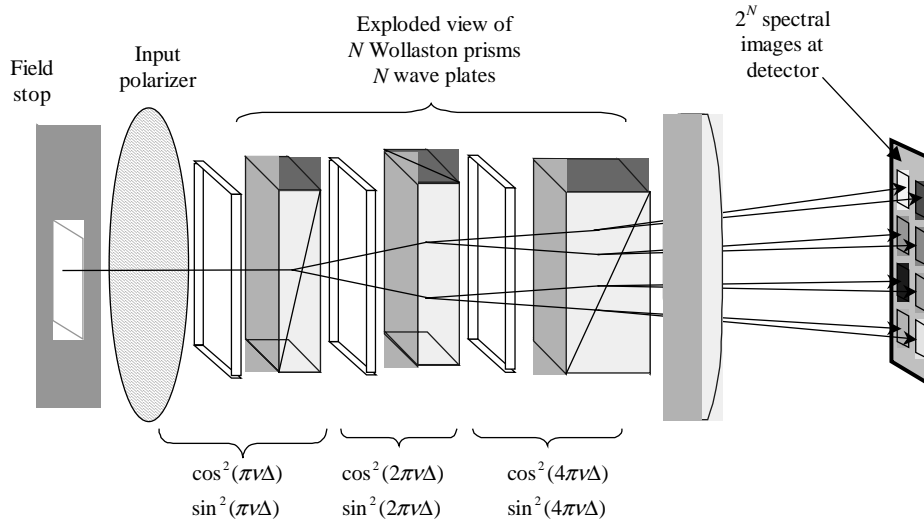


Figure 2 Depiction of principle of operation of Image replication imaging spectrometer

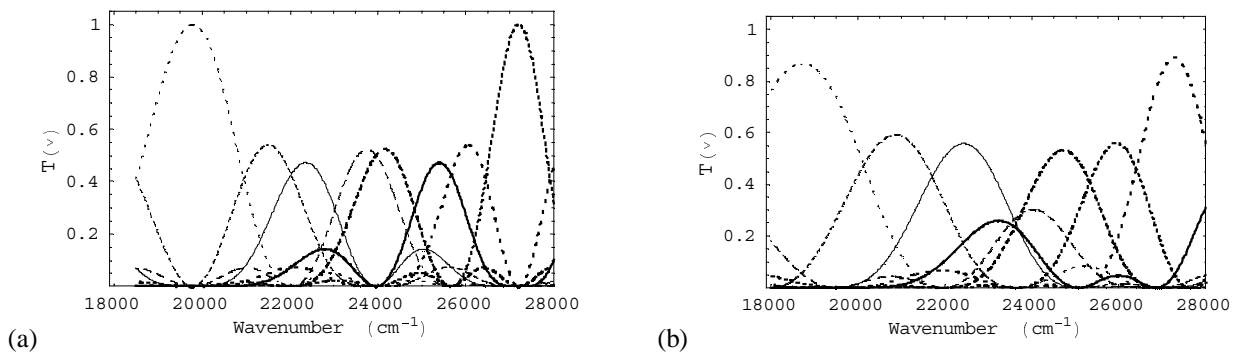


Figure 3 Transmission functions for each of eight images using (a) waveplates related by a simple factor of 2 and (b) waveplates optimised in thickness to produce transmission curves with maximum fractional power in the main lobe.

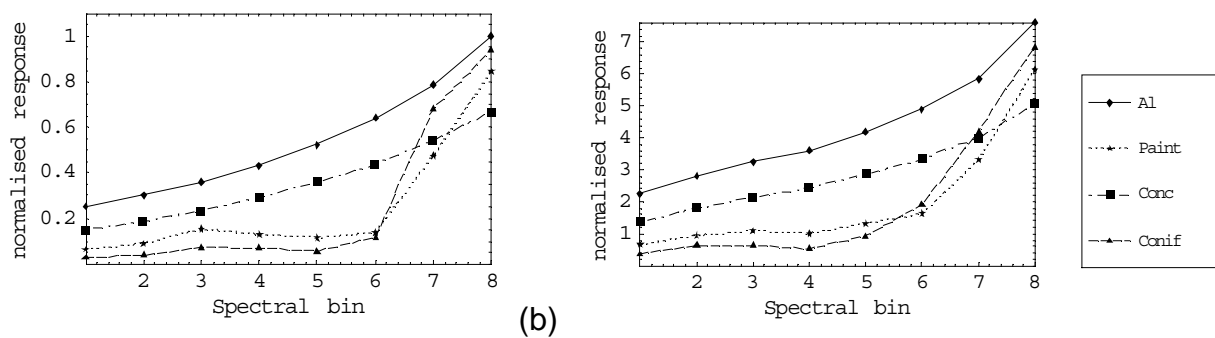


Figure 4 Spectral characterisation of spectra of aluminium, green paint, concrete and coniferous vegetation convolved with (a) rectangular filter functions and (b) IRIS optimised filter functions.

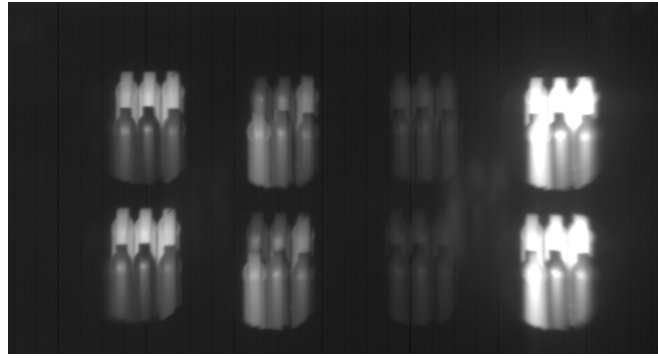


Figure 5 Replicated images of six different coloured pens at the detector plane of IRIS.

A schematic of the foveal hyperspectral imager is shown in Figure 6. The scene is imaged onto both the hyperspectral fovea and the panchromatic periphery via an intermediate focal plane. A small mirror located at the intermediate focal plane redirects light from the foveal region, via re-imaging optics, onto the image plane of the hyperspectral imager. Light not intercepted by the mirror is re-imaged onto the panchromatic detector. The hyperspectral fovea consists of an optical fibre reformatter and a commercial grating one-dimensional (1D) hyperspectral imager. The optical fibre reformatter is a coherent bundle of multimode optical fibres that reformats the foveal input plane of 14×14 pixels into a linear array of 196 output pixels that constitutes the input slit of the 1D hyperspectral imager. A spectrally dispersed image of the linear array is formed at the detector array as shown in Figure 7. Computer algorithms inverse the reformatting operation of the optical fibre reformatter to produce a 14×14 pixel hyperspectral image and integrate it with the panchromatic image prior to presentation to the user.

Subsequent to calibration, image processing algorithms can be applied to the spectral data to process the data prior to presentation to the user. In our proof-of-principle system we have employed a simple least squares recognition algorithm to identify specific spectra in the scene and to highlight them in the displayed image. This is illustrated by the sequence of still images in Figure 8 that have been extracted from a video sequence. To the naked eye, the tank and background shown in these images appear to be very similar shades of green, but when hyperspectrally imaged there are subtle differences that can be exploited. A simple spectral recognition algorithm based on a least squares fit to a target spectrum has been trained to recognise the spectrum of the tank and each pixel within the hyperspectral fovea that closely matches this spectrum is highlighted. This can be seen in the image sequence as the tank passes through the hyperspectral fovea. In these images the fovea has been intentionally darkened so that it can be discerned in the printed form. The subjective ability to use the hyperspectral fovea to identify an extended object is somewhat more enhanced than might be apparent from this image sequence; presumably because the human cognition system is highly trained at constructing representations of extended objects based on time-sequential scanning a foveal image.

In operation, one can consider the system being scanned across the scene using information cues from the panchromatic periphery to bring images of regions of interest to the hyperspectral fovea. Spectral processing algorithms operating on the data only within the fovea then enable classification of the spectra and presentation to the user in a suitable form. Suitable algorithms will enable a hyperspectral image to be 'painted' over the panchromatic periphery to assemble a hyperspectral representation of a wide field of view scene prioritised according to the importance of perceived areas of interest within it. In future embodiments the field of view of the optical fibre reformatter could be readily increased up to about 30×30 pixels using a single detector array.

4. CONCLUSIONS

All spectral imaging techniques involve some degree of compromise. Snapshot spectral imaging of transient or moving scenes generally requires either very low spectral resolution (for example, conventional colour television) or one-dimensional imaging. In this paper we have described two novel techniques that offer spectral imaging in two dimensions and are consequently well-suited to imaging of transient phenomena and for imaging from moving platforms. In addition the techniques involve no multiplexing so optical throughput is very high. Moreover, in contrast to other high throughput techniques, such as Fourier-transform spectroscopy¹, there is no data inversion and so the associated SNR advantage is retained even in shot-noise limited imaging conditions.

5. ACKNOWLEDGEMENT

This work was carried out with funding from Sensors and Electronic Warfare Research Domain of the UK MoD Corporate Research Programme

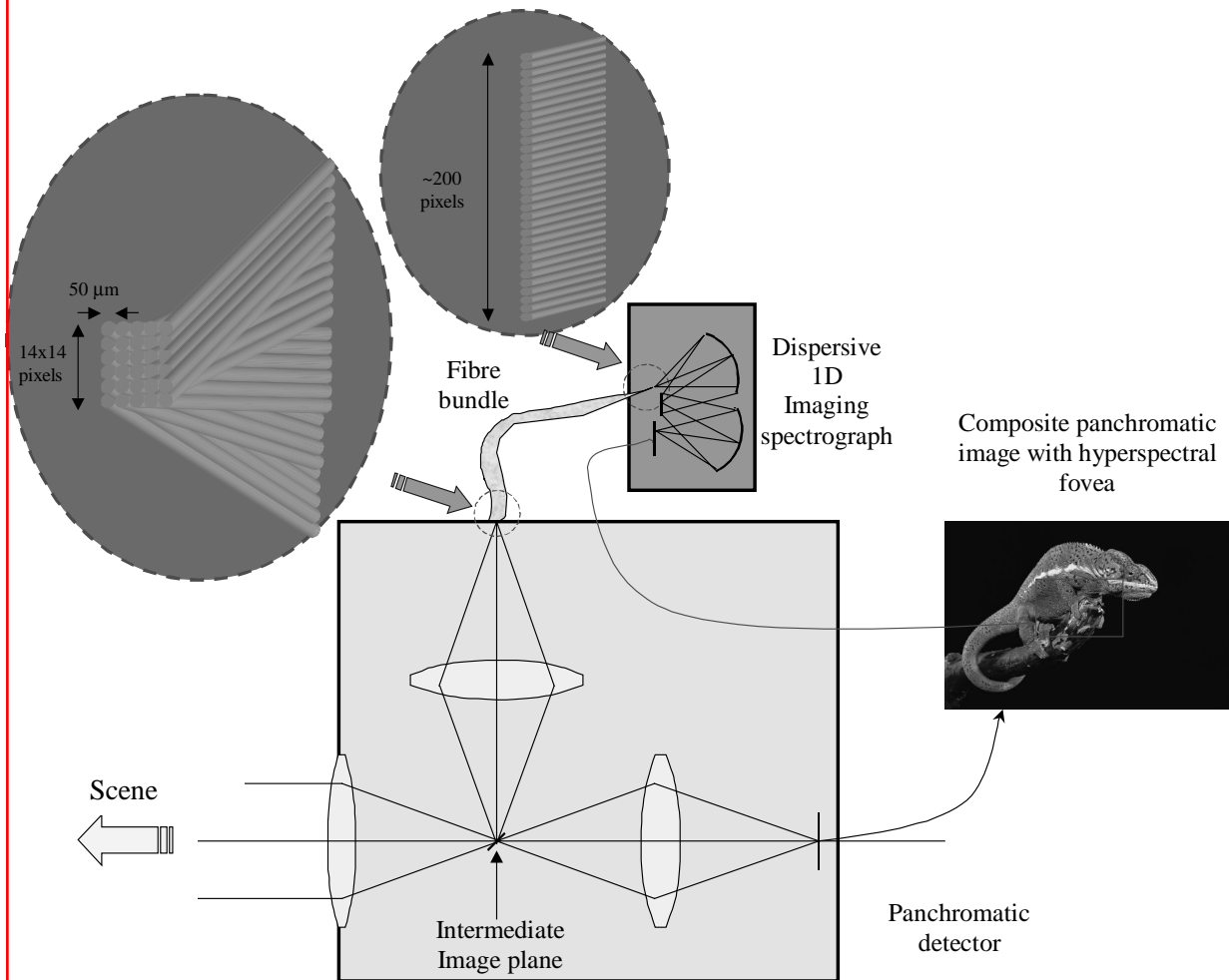


Figure 6 Schematic of the foveal hyperspectral imager

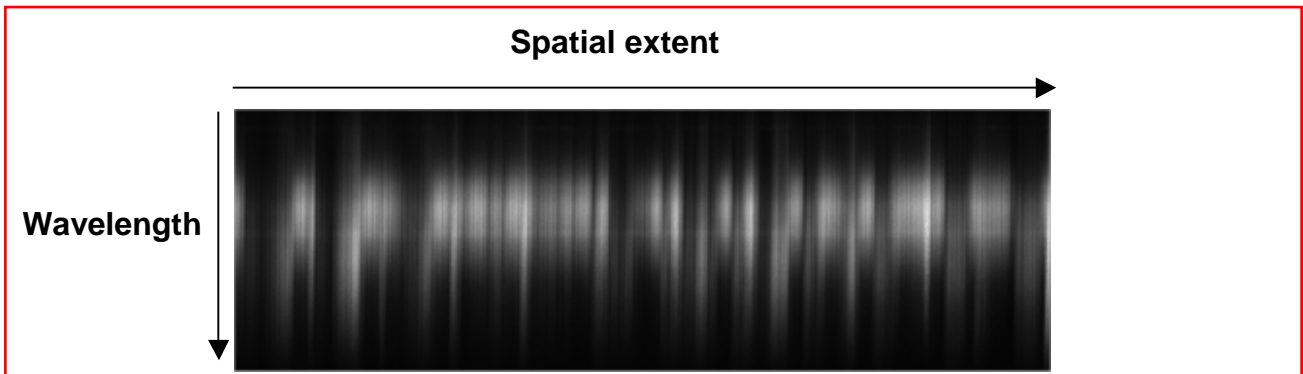


Figure 7 Image recorded at the hyperspectral fovea detector array

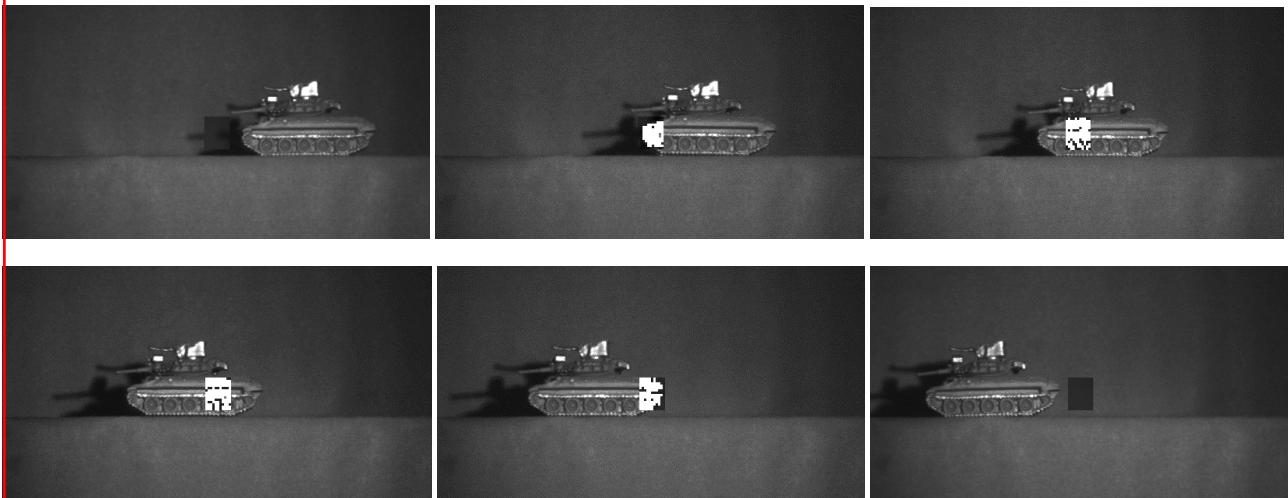


Figure 8 Foveal hyperspectral frames from a video sequence of a toy tank traversing the field of view showing the highlighting of recognised 'tank coloured' pixels.

6. REFERENCES

¹ A.R. Harvey, J. Beale, A.H. Greenaway, T.J. Hanlon and J. Williams, "Technology options for imaging spectrometry" *Proc SPIE*, 4132, pp13-24, 2000

² A R Harvey, D W Fletcher-Holmes, *Imaging apparatus*, GB Patent application 0215248.6, 2nd July 2002.

³ A.R.Harvey, J.Lawlor, A.I.McNaught, J.W.Williams and D.W.Fletcher-Holmes. *Hyperspectral imaging for the detection of retinal diseases*. SPIE 4816-37, pp325-335, Proc. Conference on Imaging Spectrometry VIII, Seattle July 7-11, 2002.

⁴ V.Papadakis, M.P. Karavellas, M.K. Tsillimbaris, C.Balas, and I.G.Pallikaris, *A hyperspectral imaging fundus camera for the detection and characterisation of retinal lesions*. The Association for Research in Vision and Ophthalmology. Ocular Imaging, 4362-B331, pp. 174, May 5-10, 2002.

⁵ J.Lawlor, D.W.Fletcher-Holmes A.I.McNaught A.R.Harvey. *In vivo hyperspectral imaging of human retina and optic disc*. The Association for Research in Vision and Development, Anatomy and Physiology/Retinal Cell Biology. 4350-B319. Annual Meeting Fort Lauderdale, Florida May 5-10, 2002

⁶ F. C.Delori, *Spectrophotometer for noninvasive measurement of intrinsic fluorescence and reflectance in the ocular fundus*, Applied Optics, Vol. 33, pp.7439-7452, 1994.

⁷ P Mouroulis, *Spectral and spatial uniformity in push-broom imaging spectrometers*, Imaging spectrometry V, SPIE 3753 pp 133-141 (1999)

- ⁸ G R O Vane, T G Green, H T Chrien, E G Hanson, W M Porter, *The airborne visible/infrared imaging spectrometer (AVRIS)* Remote Sen. Environ., **44**, pp127-143, (1993)
- ⁹ T Wilson, C Davis, *Naval EarthMap Observer (NEMO) Satellite*, Imaging Spectrometry V, SPIE 3753, pp 2-11 (1999)
- ¹⁰ J A Hackwell et al, *LWIR/MWIR imaging hyperspectral sensor for airborne and ground-based remote sensing*, Proc. SPIE 2819, pp 274-283 (1995)
- ¹¹ R W Basedow, D C Carmer, M L Anderson, *HYDICE system implementation and performance*, SPIE 2480, pp 258-267 (1995)
- ¹² B. Lyot, *Filter monochromatique polarisant et ses applications en physique solaire*, Ann. Astrophys. 7, 32 (1944)
- ¹³ B. Lyot, *Optical apparatus with wide field using interference of polarized light*, C.R. Acad. Sci. (Paris) 197, 1593 (1933).
- ¹⁴ Y. Ohman, *A new monochromator*, Nature 41, 157, 291 (1938).
- ¹⁵ Y. Ohman, *On some new birefringent filter for solar research*, Ark. Astron. 2, 165 (1958).